Supporting Information

$(C_4H_8N_5)(PhPHO_2)\cdot H_2O$: A Polar Ionic Cocrystal with Strong Second-Harmonic Generation and High Birefringence

Peng Zhuang,[abc] *Bing-Ping Yang*,*[abc] *and Jiang-Gao Mao**[abc]

[a] State Key Laboratory of Functional Crystals and Devices, Fujian Institute of Research on the Structure of Matter, Chinese Academy of Sciences, Fuzhou, 350002, P.R. China

[b] University of Chinese Academy of Sciences, Beijing, 100049, P.R. China

[c] Fujian College, University of Chinese Academy of Sciences, Fuzhou, 350002, P.R. China

E-mail: ybp@fjirsm.ac.cn

Table of Contents

Experimental Section

***Synthesis of $(C_4H_8N_5)(PhPHO_2)\cdot H_2O$ (AMTPP)*:** Phenylphosphinic acid (5.0 mmol) and 2,4-diamino-6-methyl-1,3,5-triazine (5.0 mmol) were added to a 25 mL beaker containing 15 mL of deionized water and 0.5 mL of hydrofluoric acid. The mixture was stirred at 75 °C for 20 minutes to produce a clear solution. The beaker was then placed in a fume hood, where the solution was allowed to evaporate slowly at room temperature. After approximately three days, colourless block-like crystals were obtained. The theoretical weight of the product is 1.4263 g. The mass of the obtained crystal is 1.1386 g, giving a yield of 79.8%.

***Single-Crystal X-ray Diffraction Analysis*:** Single crystal of **AMTPP** was selected and ground to appropriate dimensions. A high-quality crystal was mounted on a loop first and then mounted on a goniometer for data collection. The diffraction data for **AMTPP** was collected using Cu Kα radiation (λ = 1.54184 Å) at a temperature of 293(2) K on a Rigaku Oxford Diffraction SuperNova CCD diffractometer. Cell refinement and data reduction were performed using CrysAlisPro. Numerical absorption correction based on Gaussian integration over a multifaceted crystal model and empirical absorption correction using spherical harmonics were implemented in the SCALE3 ABSPACK scaling algorithm.[1] The structures were solved by direct methods and refined by full-matrix least-squares on F^2 using SHELXL.[2,3] All non-hydrogen atoms were refined anisotropically. The structures were checked for higher symmetry using PLATON, and no additional symmetry was found.[4] The Flack parameters were refined to 0.098(13) for **AMTPP**, confirming the correct absolute structures.[5]

Powder X-ray Diffraction: PXRD data were collected on a Rigaku MiniFlex600 diffractometer equipped with a graphite monochromator and utilizing Cu Kα radiation (λ = 1.54186 Å). Data were acquired over the 2θ range of 10–70° with a step size of 0.02°.

***Spectroscopic Measurements*:** FTIR spectra were acquired on a Bruker Vertex 70 FT-IR spectrometer in the range of 4000–400 cm^{-1} with a resolution of 2 cm^{-1} at room temperature, employing the attenuated total reflection technique. The UV-vis-NIR diffuse reflectance spectra were measured in the 200–2000 nm range using a PerkinElmer Lambda 950 spectrophotometer, with $BaSO_4$ powder serving as a 100% reflectance reference. Absorption data were derived from the diffuse reflectance data using the Kubelka-Munk function: $F(R) = (1-R)^2 / (2R) = K / S$, where K is the absorption coefficient and S is the scattering coefficient.[6] The band gap was determined by extrapolating the absorption edge to the baseline on the plot of $F(R)$ versus energy.

***Thermal Analyses*:** Thermogravimetric analysis coupled with differential thermal analysis was carried out using a NETZSCH STA 499C apparatus. Approximately 3.0 – 6.0 mg of powder was placed in an alumina crucible and heated from 25 to 800 °C at a rate of 15 °C min^{-1} under a continuous nitrogen flow.

***SHG Measurements*:** The powder SHG of the compounds was measured using a method based on that of Kurtz and Perry.[7] A Q-switched Nd:YAG laser providing 1064 nm radiation was used as the light source. The pure polycrystalline samples were ground and sieved into six particle size ranges (25–45, 45–53, 53–75, 75–109, 109–150, and 150–210 μm). Sieved KH_2PO_4 (KDP) samples with the same particle size ranges were used as references. The SHG signals for **AMTPP** and KDP within the 150–210 μm particle size range were recorded on an oscilloscope.

***Laser-induced Damage Threshold (LDT) Measurements*:** The LDT for crystalline samples of **AMTPP** and KDP were measured using a Q-switched pulsed laser (1064 nm, 10 ns, 1 Hz). Polycrystalline samples of **AMTPP** and KDP, with particle sizes ranging from 150 to 210 μm, were used for the LDT measurements. Using polycrystalline samples in LDT measurements is considered feasible because each crystallite has a diameter much larger than the wavelength of the incident laser. This means that it behaves like a macroscopic bulk material, with similar multiphoton absorption (the main process in LDT when the laser pulse width is less than 50 ps). The LDT of **AMTPP** was investigated using the R-on-1 method. In this approach, a single site on the sample is irradiated with multiple pulses. Starting from very low values, the fluence is constantly increased in steps until damage occurs.[8] The LDT was calculated using the following equation: $I = E / (\tau \times A)$, where I is the LDT value, E is the input energy at the damage point, τ is the laser pulse width, and A is the area of the circular laser spot.

***Computational Methods*:** The calculations of the electronic and optical properties were performed with the CASTEP code using the plane-wave pseudopotential density functional theory.[9,10] The GGA-PBE was chosen as the exchange correlation functional.[11] The core electron interactions were represented by the norm-conserving pseudopotential.[12] H $1s^1$, C $2s^22p^2$, N $2s^22p^3$, O $2s^22p^4$ and P $3s^23p^3$ orbital electrons were set as the valence electrons. A cutoff energy of 750 eV was used to determine of the number of plane-wave basis sets. The Monkhorst-Pack k-point samplings for numerical integration over the Brillouin zone were 2 × 1 × 4 for **AMTPP**. More than 416 empty bands were used in the optical property calculations for **AMTPP**. The calculations of the second-order nonlinear optics (NLO) susceptibilities were based on the length gauge formalism within the independent particle approximation.[13,14] The

second-order NLO susceptibility can be expressed as the following equation: $\chi_L^{abc}(-2\omega;\omega,\omega) = \chi_{inter}^{abc}(-2\omega;\omega,\omega) + \chi_{intra}^{abc}(-2\omega;\omega,\omega) + \chi_{mod}^{abc}(-2\omega;\omega,\omega)$, where the subscript L denotes the length gauge, χ_{inter}^{abc} , χ_{intra}^{abc} and χ_{mod}^{abc} give the contributions to χ_L^{abc} from interband processes, intraband processes, and the modulation of interband terms by intraband terms, respectively. To gain further understanding of the anion groups, the electronic structures of the $[C(NH_2)_3]^+$ and $(C_5H_7N_2)^+$ groups were calculated at the molecular level using the Gaussian09 package. The calculations were performed using the B3LYP functional with the 6-31G basis set, a computational setting widely validated and employed in quantum chemical calculations. The Hirshfeld surface (HS) analysis was conducted using the Crystal Explorer program, which accepts structure input files in CIF format.[15] The distances from the HS to the nearest atomic nuclei inside and outside the surface are represented by d_i and d_e respectively. The d_{norm} is the normalized contact distance, which is defined using d_i, d_e and the van der Waals radius of the atoms. The 2D-fingerprint of the HS represents a novel method for summarising the complex information contained in a molecular crystal structure into a single, unique full colour plot, which provides a 'fingerprint' of the intermolecular interactions in the crystal. Derived from the HS, these 2D-fingerprint plots provide a visual summary of the frequency of each combination of d_e and d_i across the surface of a molecule, so they not only indicate which intermolecular interactions are present, but also the relative area of the surface corresponding to each kind of interaction.

Table S1. Crystal data and structure refinement for **AMTPP**.

Empirical formula	$C_{10}H_{16}N_5O_3P$
Formula weight	285.25
Temperature [K]	293(2)
Crystal system	orthorhombic
Space group (number)	*Aba*2 (No.41)
a [Å]	10.76770(10)
b [Å]	37.5496(5)
c [Å]	6.96930(10)
α [°]	90
β [°]	90
γ [°]	90
Volume [Å^3]	2817.85(6)
Z	8
ρ_{calc} [g cm^{-3}]	1.345
μ [mm^{-1}]	1.864
F(000)	1200
Crystal size [mm^3]	0.2×0.2×0.2
Radiation	CuK_α (λ=1.54184 Å)
2θ range [°]	4.71 to 153.71 (0.79 Å)
Index ranges	$-11 \le h \le 13$, $-46 \le k \le 47$, $-8 \le l \le 8$
Reflections collected	15548
Independent reflections	2875, R_{int} = 0.0359, R_{sigma} = 0.0203
Completeness to θ = 67.684°	99.9 %
Data / Restraints / Parameters	2875 / 1 / 181
Absorption correction T_{min}/T_{max} (method)	0.5154 / 1.0000 (multi-scan)
Goodness-of-fit on F^2	1.085
Final *R* indexes [$I \ge 2\sigma(I)$]	R_1 = 0.0342, wR_2 = 0.0951
Final *R* indexes [all data]	R_1 = 0.0364, wR_2 = 0.0967
Largest peak/hole [eÅ^{-3}]	0.21/−0.19
Extinction coefficient	0.00043(12)
Flack X parameter	0.098(13)

$R_1 = \sum||F_o| - |F_c||/\sum|F_o|$, $wR_2 = \{\sum w[(F_o)^2 - (F_c)^2]^2/\sum w[(F_o)^2]^2\}^{1/2}$

Table S2. Selected bond lengths for **AMTPP**.

Bond	Bond length [Å]	Bond	Bond length [Å]
P1–O1	1.494(2)	N4–C7	1.316(3)
P1–O2	1.500(2)	N5–C8	1.306(3)
P1–C1	1.798(3)	C1–C2	1.375(5)
P1–H1A	1.35(4)	C1–C6	1.387(5)
N1–C7	1.368(3)	C2–C3	1.396(6)
N1–C9	1.357(3)	C3–C4	1.358(8)
N2–C7	1.331(3)	C5–C4	1.347(9)
N2–C8	1.345(3)	C5–C6	1.393(7)
N3–C8	1.380(3)	C9–C10	1.479(3)
N3–C9	1.298(3)		

Table S3. Selected bond angles for **AMTPP**.

Bond angle	Degree [°]	Bond angle	Degree [°]
C1–C2–C3	120.0(4)	N2–C7–N1	121.56(19)
C1–C6–C5	120.1(5)	N2–C8–N3	124.8(2)
C1–P1–H1A	103.7(15)	N3–C9–C10	120.9(2)
C2–C1–C6	118.9(4)	N3–C9–N1	122.3(2)
C2–C1–P1	121.8(3)	N4–C7–N1	117.9(2)
C4–C3–C2	119.8(5)	N4–C7–N2	120.5(2)
C4–C5–C6	119.8(5)	N5–C8–N2	119.2(2)
C5–C4–C3	121.2(5)	N5–C8–N3	116.0(2)
C6–C1–P1	119.3(3)	O1–P1–C1	109.55(14)
C7–N2–C8	116.0(2)	O1–P1–H1A	107.5(13)
C9–N1–C7	119.0(2)	O1–P1–O2	115.83(11)
C9–N3–C8	116.31(19)	O2–P1–C1	110.48(14)
N1–C9–C10	116.8(2)	O2–P1–H1A	109.1(13)

Table S4. Hydrogen bonds for **AMTPP**.

D–H···A [Å]	**d(D–H) [Å]**	**d(H···A) [Å]**	**d(D···A) [Å]**	**D–H–A [°]**
N1–H1···O1	0.86	1.73	2.586(3)	173.3
N4–H4B···O2	0.86	2.03	2.888(3)	176.7
N5–H5A···O3$^{\#1}$	0.86	2.03	2.841(4)	156.1
O3–H3A···O2	0.85	1.97	2.737(4)	149.2
O3–H3B···O2$^{\#2}$	0.85	1.98	2.816(4)	168.7

Symmetry transformations used to generate equivalent atoms:
#1: 1-X, 1-Y, +Z; #2: 0.5-X, +Y, 0.5+Z;

Table S5. Birefringence and NLO performance of phosphorus-based compounds containing π-conjugated units without metal atoms.

Compounds	Units	SHG (×KDP)	Birefringence	Ref
$(CH_6N_3)_2(CH_3PO_3)$	(CH_3PO_3)	1.0	0.053@1064 nm	[16]
$(CN_4H_7)H_2PO_2$	(H_2PO_2)	1.1	0.144@532 nm	[17]
$[NH_2(CH_2COOH)_2]H_2PO_2$	(H_2PO_2)	1.2	0.120@546 nm	[18]
$(CH_6N_3)_2HPO_3$	(HPO_3)	0.8	0.058@532 nm	[17]
$(CH_6N_3)_2PO_3F$	(PO_3F)	1.0	0.039@532 nm	[19]
$(C_5H_6N)_2B_2O(HPO_4)_2$	(PO_3OH)	0.7	0.173@546 nm	[20]
$(CH_6N_3)_2HPO_4·H_2O$	(PO_3OH)	1.2	0.014@532 nm	[21]
R-$(C_5H_{14}N_2)(HPO_4)$·H2O	(PO_3OH)	0.5	0.005@546 nm	[22]
S-$(C_5H_{14}N_2)(HPO_4)$·H2O	(PO_3OH)	0.6	0.007@546 nm	[22]
$(C_2N_4OH_7)H_2PO_3$	$[HPO_2(OH)]$	2.2	0.195@532 nm	[23]
$(C_4H_6N_3)H_2PO_3$	$[HPO_2(OH)]$	2.0	0.276@589 nm	[24]
$(CH_6N_3)H_2PO_3$	$[HPO_2(OH)]$	1.4	0.089@532 nm	[23]
$(CN_4H_7)H_2PO_3$	$[HPO_2(OH)]$	0.5	0.144@532 nm	[17]
$(C_3H_5N_2)(H_2PO_4)$	$[PO_2(OH)_2]$	0.1	0.078@546 nm	[25]
$(C_5H_6ON)H_2PO_4$	$[PO_2(OH)_2]$	3.0	0.250@1064 nm	[26]
$(C_6H_7N_2O)H_2PO_4$	$[PO_2(OH)_2]$	1.0	0.191@546 nm	[27]
$(C_3H_7N_6)_6(H_2PO_4)_4(HPO_4)$ ·$4H_2O$	$[PO_2(OH)_2]$, (PO_3OH)	0.1	0.220@1064 nm	[28]
$(C_4H_7N_2)PhHPO_3$	$PhPO_2(OH)$	0.3	N/A	[29]
AMTPP	**$(PhPHO_2)$**	**2.1**	**0.243@546 nm**	**This work**

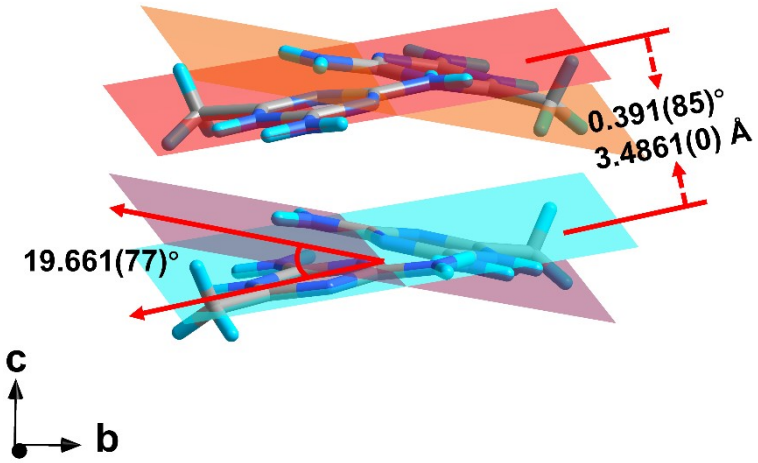

Figure S1. The arrangement of the $(C_4H_8N_5)^+$ cations.

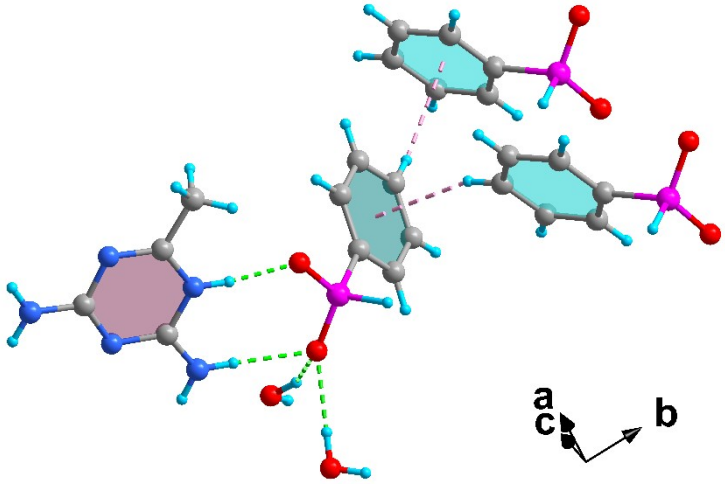

Figure S2. Hydrogen bonding and C–H···π interactions of the $(PhPHO_2)^-$ anions with surrounding $(PhPHO_2)^-$ anions, $(C_4H_8N_5)^+$ cation and water molecules in **AMTPP**.

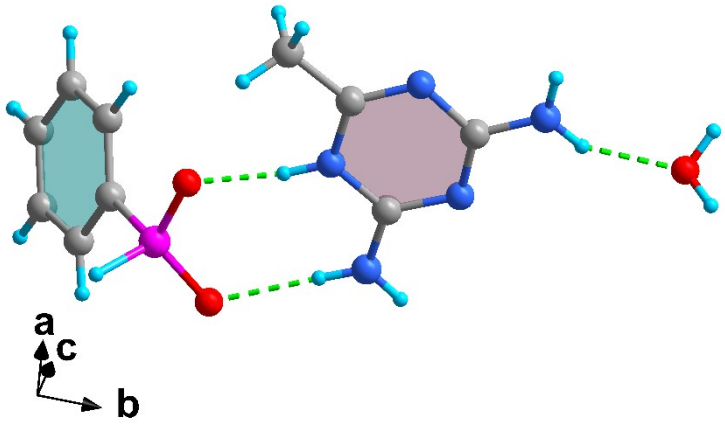

Figure S3. Hydrogen bonding interactions of the $(C_4H_8N_5)^+$ cation with surrounding $(PhPHO_2)^-$ anions and water molecule in **AMTPP**.

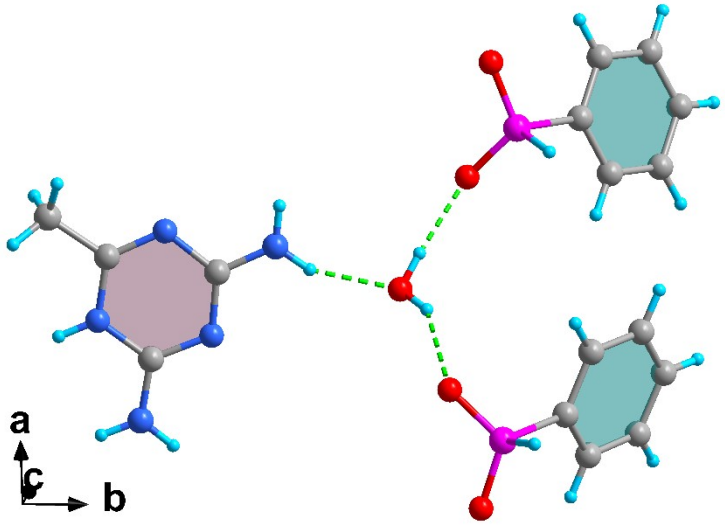

Figure S4. Hydrogen bonding interactions of the water molecule with surrounding $(PhPHO_2)^-$ anions and $(C_4H_8N_5)^+$ cation in **AMTPP**.

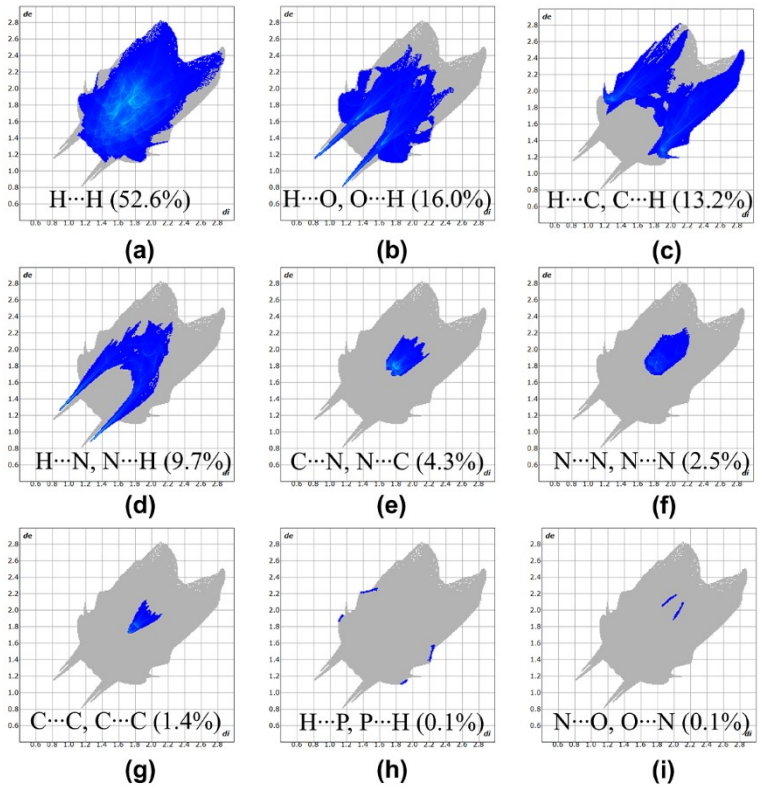

Figure S5. Fingerprint plots of the Hirshfeld surface of **AMTPP**: (a) H···H, (b) H···O, (c) H···C, (d) H···N, (e) C···N, (f) N···N, (g) C···C, (h) H···P and (i) N···O.

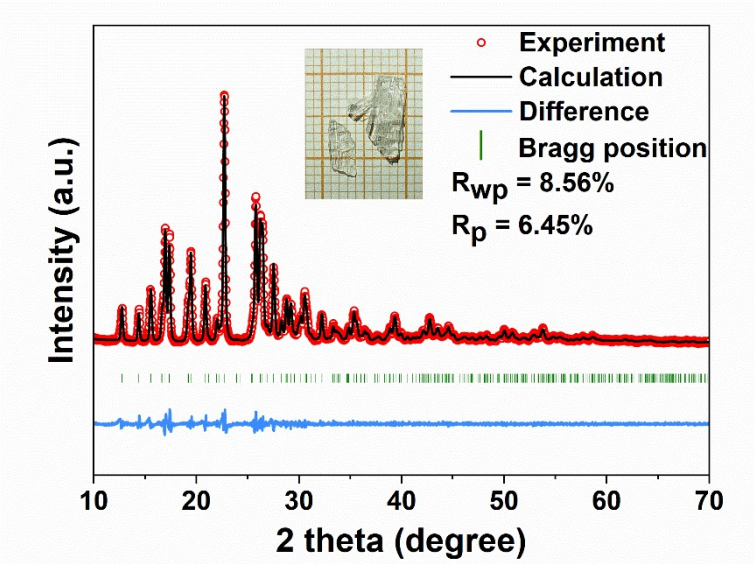

Figure S6. Refined plot and the powder XRD patterns for **AMTPP**.

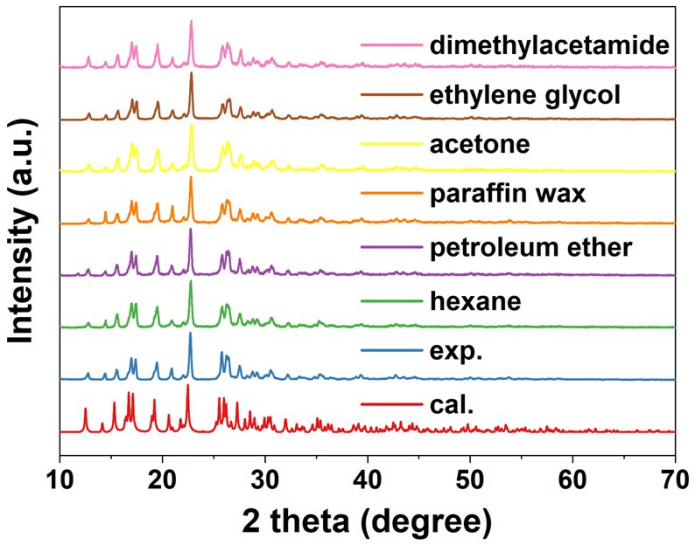

Figure S7. Experimental and calculated PXRD patterns for **AMTPP** after soaking in various organic solvents for 72 hours.

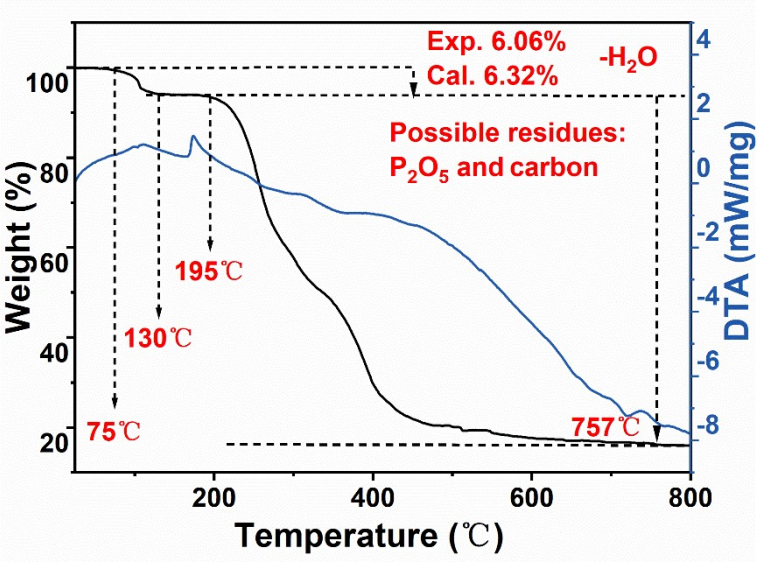

Figure S8. TGA and DTA curves for **AMTPP**.

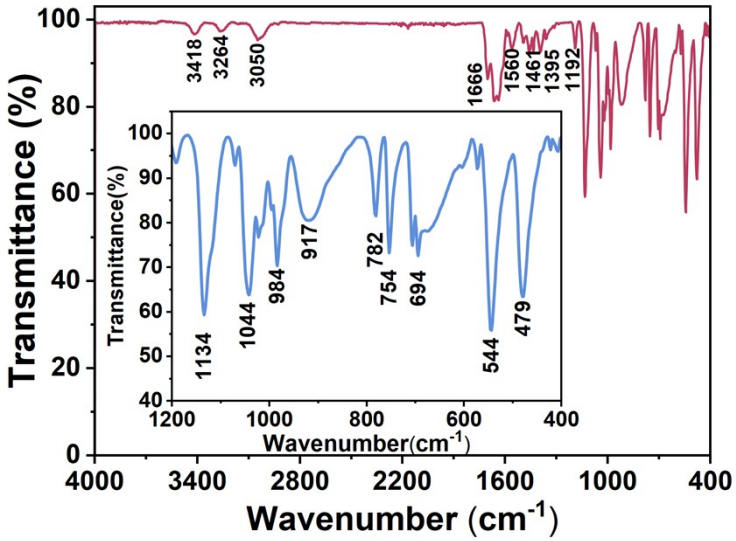

Figure S9. FTIR spectrum of **AMTPP**.

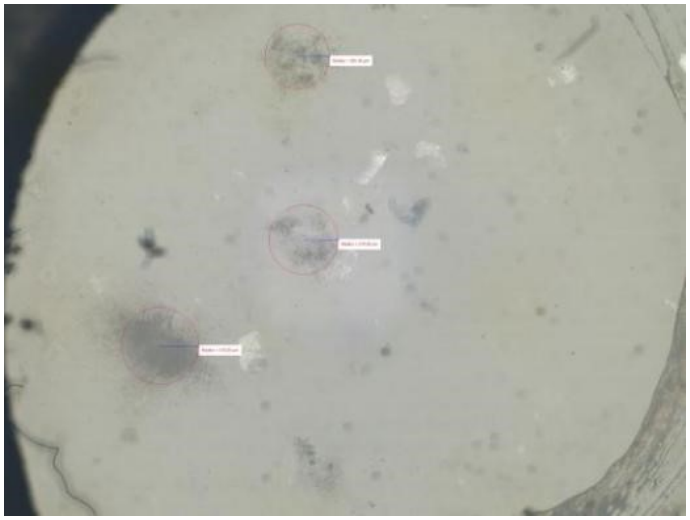

Figure S10. Optical micrograph of the laser-damaged areas on **AMTPP**.

Figure S11. Photograph of the crystals being heated in air at 150 °C for 30 minutes and then naturally cooled to room temperature.

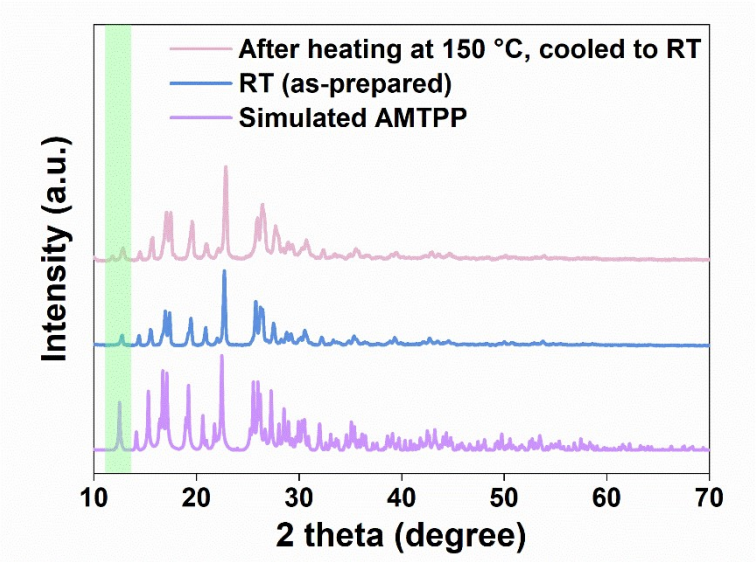

Figure S12. Simulated and experimental XRD patterns of **AMTPP** at room temperature (RT) and after treatment at 150 °C (cooled to RT).

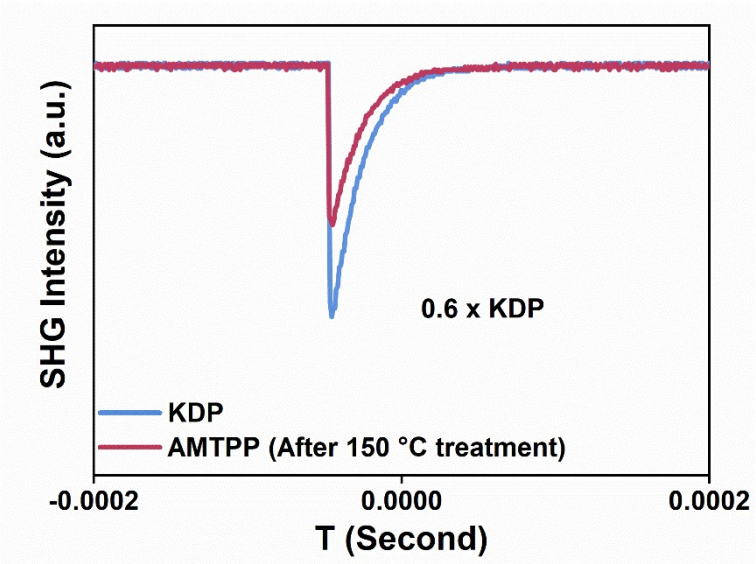

Figure S13. SHG signals of AMTPP (after treatment at 150 °C) and KDP under 1064 nm laser irradiation. Particle size: 150–210 μm.

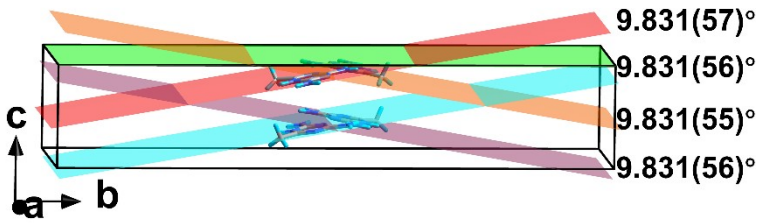

Figure S14. Dihedral angles between the $(C_4H_8N_5)^+$ cations within the unit cell and the (001) crystal plane.

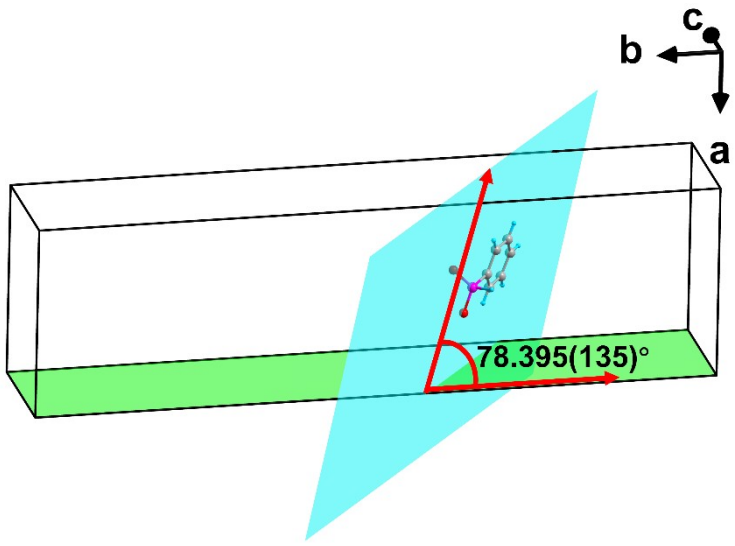

Figure S15. Dihedral angle between the $(PhPHO_2)^-$ anion in the asymmetric unit of **AMTPP** and the (100) crystal plane.

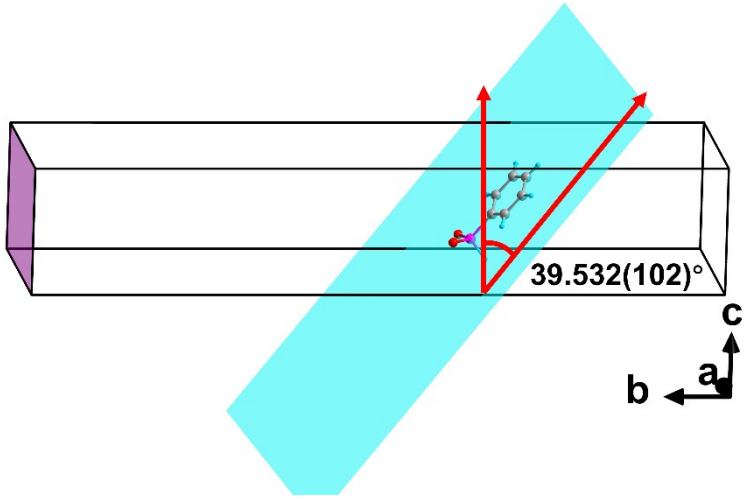

Figure S16. Dihedral angle between the $(PhPHO_2)^-$ anion in the asymmetric unit of **AMTPP** and the (010) crystal plane.

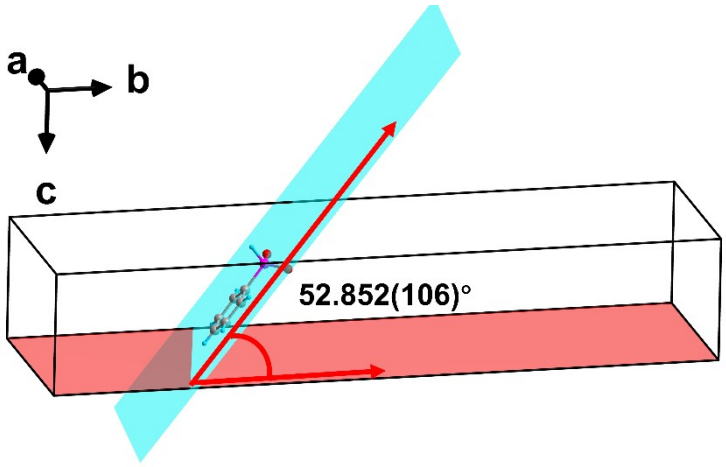

Figure S17. Dihedral angle between the $(PhPHO_2)^-$ anion in the asymmetric unit of **AMTPP** and the (001) crystal plane.

References

1 Blessing, *Acta Crystallogr., Sect. A: Found. Crystallogr.*, 1995, **51**, 33–38.
2 G. M. Sheldrick, *Acta Crystallogr. C*, 2015, **71**, 3–8.
3 G. M. Sheldrick, *Acta Crystallogr., Sect. A: Found. Adv.*, 2015, **71**, 3–8.
4 A. L. Spek, *J. Appl. Crystallogr.*, 2003, **36**, 7–13.
5 H. D. Flack, *Acta Crystallogr. Sect. A*, 1983, **39**, 876–881.
6 P. Kubelka and F. Munk, Fuer Tekn. Physik, 1931, **12**, 593-609.
7 S. K. Kurtz and T. T. Perry, *J. Appl. Phys.*, 1968, **39**, 3798–3813.
8 E. Erushin, D. Badikov, K. Anton, A. Boyko, G. Shevyrdyaeva, G. Safaraliev and N. Kostyukova, *Appl. Phys. B*, 2025, **131**:11.
9 V. Milman, B. Winkler, J. A. White, C. J. Pickard, M. C. Payne, E. V. Akhmatskaya and R. H. Nobes, *Int. J. Quantum Chem.*, 2000, **77**, 895–910.
10 M. D. Segall, P. J. D. Lindan, M. J. Probert, C. J. Pickard, P. J. Hasnip, S. J. Clark and M. C. Payne, *J. Phys.: Condens. Matter*, 2002, **14**, 2717–2744.
11 J. P. Perdew, K. Burke and M. Ernzerhof, *Phys. Rev. Lett.*, 1996, **77**, 3865–3868.
12 J. S. Lin, A. Qteish, M. C. Payne and V. Heine, *Phys. Rev. B*, 1993, **47**, 4174–4180.
13 S. Sharma, J. K. Dewhurst and C. Ambrosch-Draxl, *Phys. Rev. B*, 2003, **67**, 165332.
14 J. E. Sipe and E. Ghahramani, *Phys. Rev. B*, 1993, **48**, 11705–11722.
15 P. R. Spackman, M. J. Turner, J. J. McKinnon, S. K. Wolff, D. J. Grimwood, D. Jayatilaka and M. A. Spackman, *J. Appl. Crystallogr.*, 2021, **54**, 1006–1011.
16 S. C. Li, Y. H. Zhu, Z. L. Geng, R. B. Fu, J. L. Zeng, Y. T. Luo, S. F. Lei and Z.-J. Ma, *Mater. Chem. Front.*, 2025, **9**, 1375–1382.
17 W. B. Zhang, M. Arif, H. Zhou, R. An, Z. H. Yang, X. L. Hou, S. L. Pan and S. J. Han, *Adv. Opt. Mater.*, 2025, **13**, 2403372.
18 L. Y. Duan, X. M. Zhang, Y. Xiao, D. Q. Yang, Y. Wang and B. B. Zhang, *Adv. Opt. Mater.*, 2026, e03629.
19 L. Xiong, J. Chen, J. Lu, C.-Y. Pan and L.-M. Wu, *Chem. Mater.*, 2018, **30**, 7823–7830.
20 H. Zhang, D. Jiao, X. Li, C. He, X. Dong, K. Huang, J. Li, X. An, Q. Wei and G. Wang, *Small*, 2024, **20**, 2401464.
21 I. Němec, I. Matulková, P. Held, J. Kroupa, P. Němec, D. Li, L. Bohatý and P. Becker, *Optical Materials*, 2017, **69**, 420–431.
22 K. Huang, X.-M. Dong, C. He, Z.-X. Zhao, W. Chen, H.-Y. Zhao, J.-X. Hu, Q. Wei and G.-M. Wang, *J. Phys. Chem. Lett.*, 2025, **16**, 1881–1886.
23 G. Xu, X. Bai, Z. Yang, J. Han and S. Pan, *Angew. Chem. Int. Ed.*, 2025, e202510363.
24 Z.-P. Zhang, X. Liu, X. M. Liu, Z.-W. Lu, X. Sui, B.-Y. Zhen, Z. S. Lin, L. Chen and L.-M. Wu, *Chem. Mater.*, 2022, **34**, 1976–1984.
25 Q. Xia, X. X. Jiang, L. Qi, C. Wu, Z. S. Lin, Z. P. Huang, M. G. Humphrey, K. Tatsumi and C. Zhang, *Inorg. Chem. Front.*, 2024, **11**, 8813–8823.
26 J. Lu, X. Liu, M. Zhao, X.-B. Deng, K.-X. Shi, Q.-R. Wu, L. Chen and L.-M. Wu, *J. Am. Chem. Soc.*, 2021, **143**, 3647–3654.
27 M.-B. Xu, J. Chen, H.-Y. Wu, J.-J. Li, N. Yu, M.-F. Zhuo, F.-F. Mao and K.-Z. Du, *Inorg. Chem. Front.*, 2024, **11**, 4307–4317.
28 S.-F. Li, L. Hu, Y. Ma, F.-F. Mao, J. Zheng, X.-D. Zhang and D. Yan, *Inorg. Chem.*, 2022, **61**, 10182–10189.
29 J. Fuller and N. E. Heimer, *J. Chem. Crystallogr.*, 1995, **25**, 129–136.